Spin-dependent transport through a Weyl semimetal surface

V. D. Esin, D. N. Borisenko, A. V. Timonina, N. N. Kolesnikov, and E. V. Deviatov
Institute of Solid State Physics of the Russian Academy of Sciences, Chernogolovka, Moscow District, 2 Academician Ossipyan str. 142432, Russia

(Received 7 February 2020; accepted 7 April 2020; published 24 April 2020)

We experimentally compare two types of interface structures with magnetic and nonmagnetic Weyl semimetals. They are the junctions between a gold normal layer and magnetic Weyl semimetal Ti_2MnAl, and a ferromagnetic nickel layer and nonmagnetic Weyl semimetal WTe_2, respectively. Due to the ferromagnetic side of the junction, we investigate spin-polarized transport through the Weyl semimetal surface. For both structures, we demonstrate similar current-voltage characteristics, with hysteresis at low currents and sharp peaks in differential resistance at high ones. Despite this behavior resembling the known current-induced magnetization dynamics in ferromagnetic structures, evolution of the resistance peaks with magnetic field is unusual. We connect the observed effects with current-induced spin dynamics in Weyl topological surface states.

DOI: 10.1103/PhysRevB.101.155309

I. INTRODUCTION

Recent interest in topological semimetals is connected with their peculiar properties [1], which originate from gapless spectrum with band touching in some distinct points. In Weyl semimetals (WSM) every touching point splits into two Weyl nodes with opposite chiralities due to the time reversal or inversion symmetries breaking. The projections of two Weyl nodes on the surface Brillouin zone are connected by a Fermi arc, which represents the topologically protected surface state [1]. Most of experimentally investigated WSMs were noncentrosymmetric crystals with broken inversion symmetry [1]. For example, spin- and angle-resolved photoemission spectroscopy data indeed demonstrate spin-polarized surface Fermi arcs [2,3] for a WTe_2 Weyl semimetal [4,5]. In contrast, there are only a few candidates of magnetically ordered materials for the realization of WSMs [6–11].

Ti_2MnAl is one of the newly predicted [12,13] magnetic WSM. The bulk Ti_2MnAl is a spin gapless semiconductor, where the valence and conduction bands touch each other in the spin-up channel and there is a large gap in the spin-down band structure [14]. Therefore, the bulk Ti_2MnAl has 100% spin-polarized carriers.

It is well known that the magnetically ordered materials allow complicated magnetization dynamics. For example, current-induced excitation of spin waves, or magnons, was demonstrated as sharp dV/dI differential resistance peaks in ferromagnetic multilayers at large electrical current densities [15–21]. In these structures, spin-dependent scattering may even reverse the magnetic moments of the layers, which results in dV/dI switchings at low currents, accomplished by well-defined hysteresis [15].

Bulk magnons were also demonstrated [22] for magnetic WSM at low current densities due to the coupling between two magnetic moments mediated by Weyl fermions [23]. Also, in a bilayer consisting of a magnetic WSM and a normal metal, a charge current can be induced in the WSM by spin current injection at the interface [24]. On the other hand, there are spin-polarized surface Fermi arcs on a WSM surface [2,3,25–27]. Similarly to the case of topological insulators [28], one can expect current-induced magnetization dynamics [29] also for surface magnetic textures [30,31] in WSM.

Here, we experimentally compare two types of interface structures with magnetic and nonmagnetic Weyl semimetals. They are the junctions between a gold normal layer and magnetic Weyl semimetal Ti_2MnAl, and a ferromagnetic nickel layer and nonmagnetic Weyl semimetal WTe_2, respectively. Due to the ferromagnetic side of the junction, we investigate spin-polarized transport through the Weyl semimetal surface. For both structures, we demonstrate similar current-voltage characteristics, with hysteresis at low currents and sharp peaks in differential resistance at high ones. Despite this behavior resembling the known current-induced magnetization dynamics in ferromagnetic structures, evolution of the resistance peaks with magnetic field is unusual. We connect the observed effects with current-induced spin dynamics in Weyl topological surface states.

II. SAMPLES AND TECHNIQUE

Ti_2MnAl was obtained as a bulk ingot by levitation melting in high-frequency (60–70 kHz) induction furnace. A mixture of Mn and Al powders was placed into the cylindrical titanium capsule and melted in a suspended condition for 20 min in argon medium at 0.2 MPa pressure and at 2080 K temperature. After switching the heater off the resulting globule of the melt was dropped to a cooled copper crystallizer, where it was quenched at 278 K. The ingot cleaved mechanically for further processing as shown in Figs. 1(a) and 1(b). We check by standard magnetoresistance measurements that our Ti_2MnAl is characterized by low positive magnetoresistance, see Fig. 1(c), which has been demonstrated for this material [14].

The WTe_2 compound was synthesized from elements by reaction of metal with tellurium vapor in the sealed silica ampule. The WTe_2 crystals were grown by the two-stage

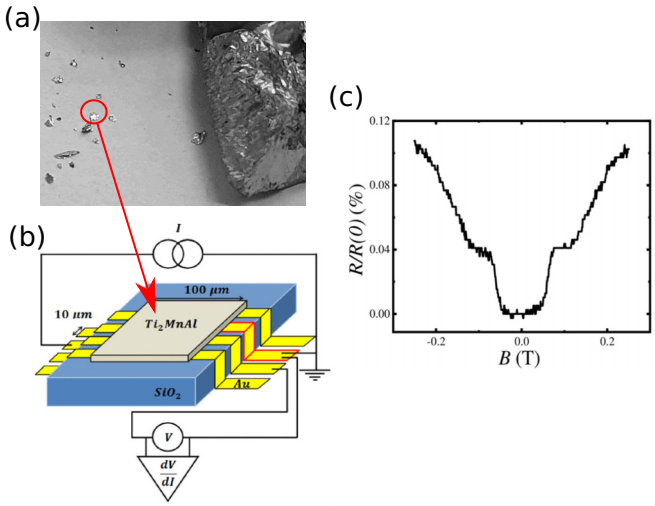

FIG. 1. (a) An initial Ti_2MnAl drop (right) and cleaved flakes (left). (b) The sketch of a sample with electrical connections. 100 nm thick and 10 μm wide Au leads are formed on a SiO_2 substrate. A Ti_2MnAl flake [$\approx 100\,\mu$m size, denoted by red circle in (a)] is transferred on top of the leads with $\approx 10\,\mu$m overlap, forming planar Au-Ti_2MnAl junctions. Charge transport is investigated with a standard three-point technique: the studied contact (denoted by the red border) is grounded and two other contacts are used for applying current and measuring potential. (c) The bulk Ti_2MnAl material demonstrates low positive magnetiresistance which coincide even quantitatively with the known one [14] for this material.

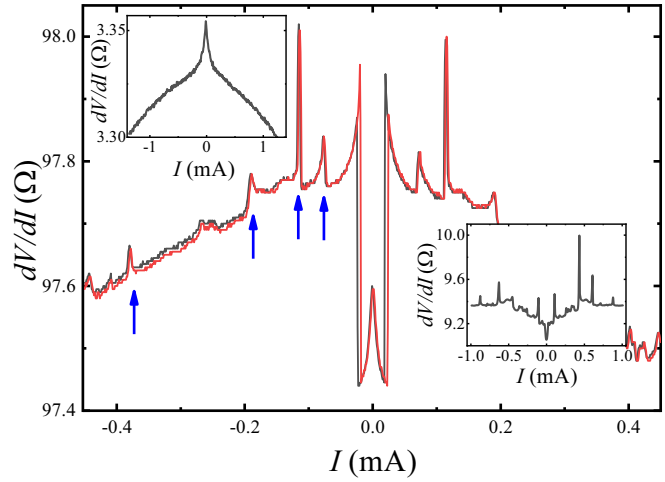

FIG. 2. Typical examples of $dV/dI(I)$ curves for transport across Au-Ti_2MnAl interface for two opposite current sweep directions. Low-current switchings of dV/dI at $\approx \pm 25\mu$A bias show well-defined hysteresis. Also, there are sharp dV/dI peaks at high currents, the peaks' positions are independent of the sweep direction. These dV/dI features originate from Au-Ti_2MnAl interface, since no dV/dI specifics can be observed by four-point measurements for bulk Ti_2MnAl, as depicted in the left inset. The right inset demonstrates similar $dV/dI(I)$ behavior for Ni-WTe_2 interface. The curves are obtained at 30 mK in zero magnetic field.

iodine transport [32], which previously was successfully applied [32,33] for growth of other metal chalcogenides such as NbS_2 and $CrNb_3S_6$. The WTe_2 composition is verified by energy-dispersive x-ray spectroscopy. The x-ray diffraction (Oxford diffraction Gemini-A, MoKα) confirms $Pmn2_1$ orthorhombic single-crystal WTe_2 with lattice parameters $a = 3.4875$ Å, $b = 6.2672$ Å, and $c = 14.0630$ Å. We check that our WTe_2 crystals demonstrate large (about 3000%), nonsaturating positive magnetoresistance up to 14 T field, as it has been shown [34,35] for WTe_2 and is expected [25–27] for nonmagnetic type-II Weyl semimetals [4].

We prepare two types of interface structures. One of them is the junction between a gold normal layer and a magnetic Weyl semimetal Ti_2MnAl, see Fig. 1(b). The other one is the junction [36] between a ferromagnetic nickel layer and a nonmagnetic Weyl semimetal WTe_2. In both cases, 50 nm thick metallic film (nickel or gold) is thermally evaporated on the insulating SiO_2 substrate. For nickel evaporation, the substrate is mounted on the in-plane magnetized sample holder. 10 μm wide metallic leads are formed by photolithography and lift-off technique. Small (about 100 μm size and 1 μm thick) WTe_2 flakes can be easily obtained from layered WTe_2 single crystals. For Ti_2MnAl, flakes are obtained by a mechanical cleaving method, see Fig. 1(a). Then we select the most plane-parallel Ti_2MnAl flakes with clean surface, where no surface defects could be resolved with optical microscope. A single flake (WTe_2 or Ti_2MnAl) is transferred on top of the metallic leads with $\approx 10 \times 10\,\mu m^2$ overlap and pressed slightly with another oxidized silicon substrate. A special metallic frame allows us to keep the substrates parallel and apply a weak pressure to the sample. No external pressure is needed for a flake to hold on to a substrate with metallic leads afterward. This procedure provides transparent Ni-WTe_2 or Au-Ti_2MnAl junctions, stable in different cooling cycles, which has been also demonstrated before [36–38].

We investigate transport properties of a single Ni-WTe_2 or Au-Ti_2MnAl junction by a three-point technique, see Fig. 1(b): a studied contact is grounded, two other contacts are employed to apply current I and measure voltage V, respectively. To obtain $dV/dI(I)$ characteristics, the dc current I is additionally modulated by a low ac component ($\approx 2\,\mu$A, $f = 2$ kHz). We measure both dc (V) and ac (which is proportional to dV/dI) components of the voltage drop with a dc volt meter and a lock in, respectively. Measured ac signal is independent of frequency in 1–5 kHz range, which is defined by applied ac filters. In the connection scheme in Fig. 1(b), all the wire resistances are excluded, which is necessary for low-impedance samples. The measurements are performed in a dilution refrigerator for the temperature interval 30 mK–1.2 K for two different orientations of the magnetic field to the interface. To ensure the homogeneous magnetic state of the junctions, the magnetization procedure is performed: an external magnetic field is swept slowly from zero to 5 T, afterward, the external field goes down to zero.

III. EXPERIMENTAL RESULTS

Figure 2 provides typical examples of low-temperature $dV/dI(I)$ characteristics for Au-Ti_2MnAl (in the main field) and Ni-WTe_2 (in the right inset) junctions. Despite different materials, we observe similar qualitative behavior for both types of the interfaces: $dV/dI(I)$ curves are nonlinear,

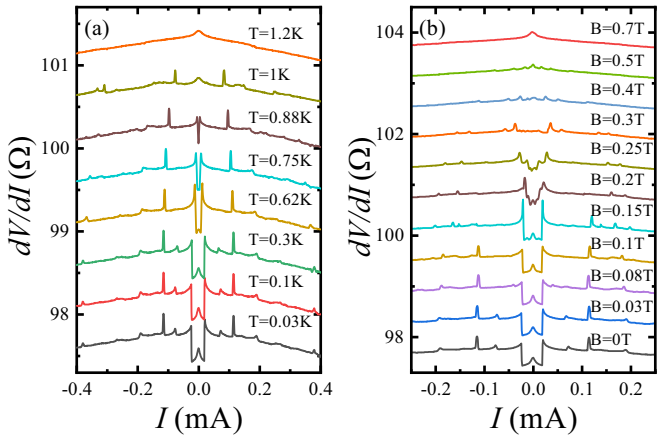

FIG. 3. Evolution of $dV/dI(I)$ characteristics of the Au-Ti_2MnAl junction with (a) temperature and (b) parallel to the interface magnetic field. The curves are shifted for clarity. All dV/dI features are suppressed above 1 K or 0.5 T, respectively, they also demonstrate a complicated evolution. The curves in (a) are obtained in zero magnetic field, the ones in (b) are at 30 mK.

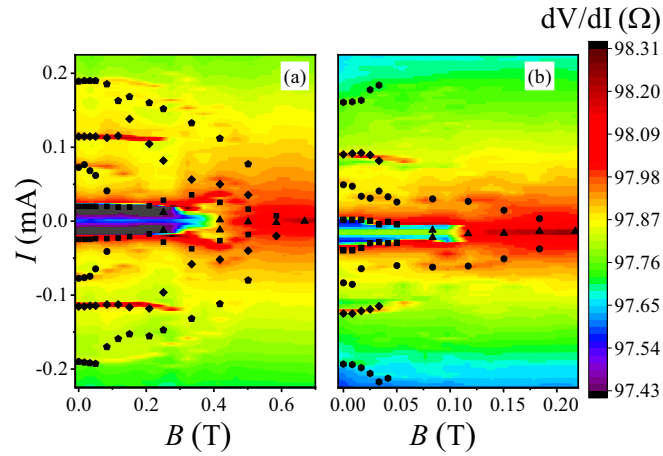

FIG. 4. Evolution of dV/dI peaks' positions for Au-Ti_2MnAl junction for (a) parallel and (b) normal to the interface magnetic fields. dV/dI peaks are shifting to lower currents with the field increase. Full peaks' suppression can be seen at ≈0.6 T for the parallel field orientation, but it occurs much earlier, at ≈0.2 T, for the normal one. The data are obtained for 30 mK temperature.

there are dV/dI peaks at high currents, and sharp symmetric switchings of differential resistance at low, $\approx \pm 25$ μA bias. The peaks' positions are independent of the current sweep direction, while dV/dI switchings at $\approx \pm 25$ μA demonstrates well-defined hysteresis.

We should connect the observed dV/dI features with interface effects. In a three-point technique, the measured potential V reflects in-series connected resistances of the Ni-WTe_2 or Au-Ti_2MnAl interface and some part of the crystal flake. From $dV/dI(I)$ independence of the particular choice of current and voltage probes in Fig. 1(b), we verify that the interface resistance dominates in the obtained $dV/dI(I)$ curves. Also, we do not observe any dV/dI features in bulk properties of Ti_2MnAl, which is demonstrated by four-point measurements in the left inset to Fig. 2.

The obtained dV/dI features can be suppressed by temperature or magnetic field above 1 K or 0.5 T, respectively, see Fig. 3. The positions of both the peaks and resistance switchings are moving to zero current with temperature increase until complete disappearance at 1.2 K, as depicted in Fig. 3(a). Evolution of $dV/dI(I)$ curves with magnetic field is different: the width of the low-current region (≈50 μA) is nearly independent of the magnetic field, while the dV/dI switching amplitude is gradually diminishing with the field. In contrast, dV/dI peaks' positions move to zero in a complicated manner.

The detailed behavior of dV/dI peaks' positions is shown in Fig. 4 for Au-Ti_2MnAl junction for parallel [Fig. 4(a)] and normal [Fig. 4(b)] to the interface magnetic fields. For both field orientations, the positions of the peaks are shifting nonmonotonously to smaller currents, so the peaks disappears above some value of magnetic field. This value is significantly smaller for the normal field orientation [≈0.2 T, see Fig. 4(b)], in comparison with ≈0.6 T for the parallel one [Fig. 4(a)].

To our surprise, not only $dV/dI(I)$ curves are similar for Ni-WTe_2 and Au-Ti_2MnAl interfaces in Fig. 2, but also dV/dI features show analogous behavior. For Ni-WTe_2, dV/dI peaks' positions are shifting to zero current with magnetic field, the suppression is twice faster in normal field, see Fig. 5.

IV. DISCUSSION

As a result, both Au-Ti_2MnAl and Ni-WTe_2 junctions demonstrate similar $dV/dI(I)$ characteristics, with hysteresis at low currents and sharp peaks at high ones. Moreover, we observe qualitatively similar evolution of the peaks' positions with magnetic field for both structures in Figs. 4 and 5. For this reason, the obtained results should have the same origin for these structures. From the experimental point of

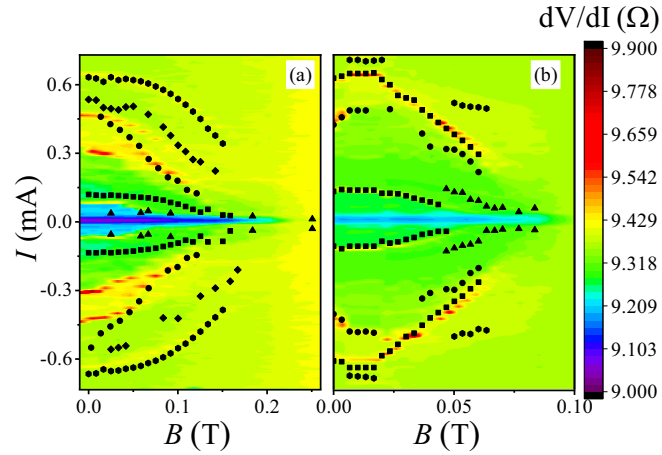

FIG. 5. Evolution of dV/dI peaks' positions for Ni-WTe_2 junction also for (a) parallel and (b) normal to the interface magnetic fields. The behavior is qualitatively similar to the Au-Ti_2MnAl case in Fig. 4. dV/dI peaks are suppressed at ≈0.2 T for the parallel field orientation, the suppression is twice faster in normal fields. The data are obtained for 30 mK temperature.

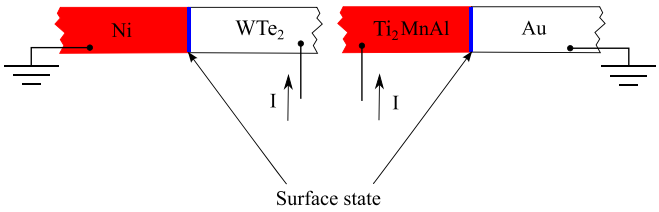

FIG. 6. Schematic representation of Au-Ti_2MnAl and Ni-WTe_2 interfaces, which are characterized by Weyl surface states at the interface (blue color). In every case, one side of the junction has significant net spin polarization of carriers (Ni or Ti_2MnAl, respectively, red color). Thus, spin-dependent transport through the Weyl surface state is investigated for these junctions.

view, the obtained $dV/dI(I)$ curves are similar to ones for ferromagnetic multilayers [15–21].

The Weyl surface state is the only common characteristic [1–3,12] of Au-Ti_2MnAl and Ni-WTe_2 interfaces, since the materials are completely different for the metallic contacts and the semimetals itself: for Au-Ti_2MnAl junction we study transport between a magnetically-ordered WSM and a normal metal, while Ni-WTe_2 one represents the junction between a nonmagnetic WSM and a ferromagnet, see Fig. 6. Also, strong temperature dependence in the 30 mK–1.2 K range can only originate from the surface, since transport properties of Ni or Au layers and bulk WSM [14,35] are invariant in this temperature range.

For Au-Ti_2MnAl and Ni-WTe_2 samples, one side of the junction has significant net spin polarization of carriers (Ni or Ti_2MnAl, respectively). We should conclude that similar $dV/dI(I)$ curves are produced by spin-polarized transport through the Weyl surface state at the interface. In some sense, our experiment resembles ones on ferromagnetic multilayers, where spin-dependent scattering affects the magnetic moments of the spin-polarized layers, while their mutual orientation defines the differential resistance [15–21]. It might be natural [28,29] that we observe similar $dV/dI(I)$ characteristics.

Let us start from dV/dI switchings at low currents in Fig. 2. At zero bias, one can expect that spin polarization of some carriers at the WSM surface is aligned parallel to one in the ferromagnet due to the complicated spin texture [30,31] on the Weyl surface [2,3,25,26]. For this reason, even spin-polarized carriers have a direct transport channel, which is reflected in low junction resistance at zero bias. While increasing the current through the junction, spin-momentum locking produces [29,31] a preferable spin polarization in the surface state, which is reflected as sharp dV/dI increase for both signs of the current. As usual [15], current-induced switchings are accompanied by hysteresis in Fig. 2. Spin alignment disappears at zero bias, when high magnetic field or temperature destroys the spin textures in the topological surface state, see Figs. 3(a) and 3(b).

Similarly to the ferromagnetic multilayers [16,17], we should identify dV/dI peaks in Fig. 2 as the onset of the current-driven magnon excitations. However, evolution of the peaks' positions with magnetic field is unusual: the peaks are moving to lower currents in Figs. 4 and 5, which is opposite to the known bulk magnon behavior [15–22]. This peaks' evolution is the main difference of our results from the standard magnon experiments [15–22].

Since the peaks disappear simultaneously with dV/dI switchings in Figs. 3(a) and 3(b), we should also connect [28] the magnon excitation with spin textures [30,31] in the topological surface states. In general, the dV/dI peak position I_{sw} is described by Slonczewski model [18,39]. Slightly simplified,

$$I_{sw}(H) \sim \alpha\gamma e\sigma H, \tag{1}$$

where α is the damping parameter, γ is the gyromagnetic ratio, σ is the total spin of the free layer. In contrast to multilayers, the total spin σ is not a constant. It is diminishing to zero when high magnetic field or temperature destroys the spin textures in the topological surface state. This $\sigma(H,T)$ dependence can be the origin of the unusual peaks' evolution in Figs. 3, 4, and 5. However, we have no complete description of the magnon dynamics in Weyl topological surface states, in contrast to the case of topological insulators [28].

It is well known that surface state transport can be observed only at temperatures that are significantly lower than the temperature of the corresponding spectrum gap. For example, for the quantum Hall effect, temperatures below 1 K were necessary to see the edge state transport [40–42]. The same situation is for topological insulators [43,44]. For Weyl semimetals, we also observed [38] Weyl specifics in Andreev reflection only below 1 K, while the Nb gap was estimated as about 10 K in this experiment. Strong temperature dependence in Fig. 3(a) is in a contrast with known bulk behavior [15–22], which can also indicate the surface state origin of the observed peaks.

V. CONCLUSION

As a conclusion, we experimentally compare two types of interface structures with magnetic and nonmagnetic Weyl semimetals. They are the junctions between a gold normal layer and magnetic Weyl semimetal Ti_2MnAl, and a ferromagnetic nickel layer and nonmagnetic Weyl semimetal WTe_2, respectively. Due to the ferromagnetic side of the junction, we investigate spin-polarized transport through the Weyl semimetal surface. For both structures, we demonstrate similar current-voltage characteristics, with hysteresis at low currents and sharp peaks in differential resistance at high ones. Despite this behavior resembling the known current-induced magnetization dynamics in ferromagnetic structures, evolution of the resistance peaks with magnetic field is unusual. We connect the observed effects with current-induced spin dynamics in Weyl topological surface states.

ACKNOWLEDGMENTS

We wish to thank V. T. Dolgopolov for fruitful discussions, S. S. Khasanov for x-ray sample characterization, A. A. Kononov and O. O. Shvetsov for help with experiment. We gratefully acknowledge financial support partially by the RFBR (Project No. 19-02-00203), RAS, and RF State task.

[1] As a recent review see N. P. Armitage, E. J. Mele, and A. Vishwanath, Rev. Mod. Phys. **90**, 015001 (2018).

[2] P. K. Das, D. D. Sante, I. Vobornik, J. Fujii, T. Okuda, E. Bruyer, A. Gyenis, B. E. Feldman, J. Tao, R. Ciancio, G. Rossi, M. N. Ali, S. Picozzi, A. Yadzani, G. Panaccione, and R. J. Cava, Nature Commun. **7**, 10847 (2016).

[3] B. Feng, Y.-H. Chan, Y. Feng, R.-Y. Liu, 1 M.-Y. Chou, K. Kuroda, K. Yaji, A. Harasawa, P. Moras, A. Barinov, W. Malaeb, C. Bareille, T. Kondo, S. Shin, F. Komori, T.-C. Chiang, Y. Shi, and I. Matsuda, Phys. Rev. B **94**, 195134 (2016).

[4] P. Li, Y. Wen, X. He1, Q. Zhang, C. Xia, Z.-M. Yu, S. A. Yang, Z. Zhu, H. N. Alshareef, and X.-X. Zhang, Nature Commun. **8**, 2150 (2017).

[5] A. A. Soluyanov, D. Gresch, Z. Wang, Q. Wu, M. Troyer, X. Dai, and B. A. Bernevig, Nature (London) **527**, 495 (2015).

[6] X. Wan, A. M. Turner, A. Vishwanath, and S. Y. Savrasov, Phys. Rev. B **83**, 205101 (2011).

[7] M. Hirschberger, S. Kushwaha, Z. Wang, Q. Gibson, S. Liang, C. A. Belvin, B. A. Bernevig, R. J. Cava, and N. P. Ong, Nature Mater. **15**, 1161-1165 (2016).

[8] G. Xu, H. Weng, Z. Wang, X. Dai, and Z. Fang, Phys. Rev. Lett. **107**, 186806 (2011).

[9] S. K. Kushwaha, Z. Wang, T. Kong, and R. J. Cava, J. Phys.: Condens. Matter. **30**, 075701 (2018).

[10] E. Liu, Y. Sun, N. Kumar, L. Muechler, A. Sun, L. Jiao, S.-Y. Yang, D. Liu, A. Liang, Q. Xu, J. Kroder, V. Süss, H. Borrmann, C. Shekhar, Z. Wang, C. Xi, W. Wang, W. Schnelle, S. Wirth, Y. Chen, S. T. B. Goennenwein, and C. Felser, Nature Phys. **14**, 1125 (2018).

[11] Q. Wang, Y. Xu, R. Lou, Z. Liu, M. Li, Y. Huang, D. Shen, H. Weng, S. Wang and H. Lei, Nature Commun. **9**, 3681 (2018).

[12] W. Shi, L. Muechler, K. Manna, Y. Zhang, K. Koepernik, R. Car, J. van den Brink, C. Felser, and Y. Sun, Phys. Rev. B **97**, 060406(R) (2018).

[13] L. Wollmann, A. K. Nayak, S. S. P. Parkin, and C. Felser, Annu. Rev. Mater. Res. **47**, 247 (2017).

[14] W. Feng, X. Fu, C. Wan, Z. Yuan, X. Han, N. Van Quang, and S. Cho, Phys. Status Solidi RRL **9**, 641 (2015);

[15] E. B. Myers, D. C. Ralph, J. A. Katine, R. N. Louie, and R. A. Buhrman, Science **285**, 867 (1999).

[16] M. Tsoi, A. G. M. Jansen, J. Bass, W.-C. Chiang, M. Seck, V. Tsoi, and P. Wyder, Phys. Rev. Lett. **80**, 4281 (1998).

[17] M. Tsoi, A. G. M. Jansen, J. Bass, W.-C. Chiang, V. Tsoi, and P. Wyder, Nature (London) **406**, 46 (2000).

[18] J. A. Katine, F. J. Albert, R. A. Buhrman, E. B. Myers, and D. C. Ralph, Phys. Rev. Lett. **84**, 3149 (2000).

[19] Y. Ji, C. L. Chien, and M. D. Stiles, Phys. Rev. Lett. **90**, 106601 (2003).

[20] O. P. Balkashin, V. V. Fisun, I. K. Yanson, L. Yu. Triputen, A. Konovalenko, and V. Korenivski, Phys. Rev. B **79**, 092419 (2009).

[21] T. Balashov, A. F. Takács, M. Däne, A. Ernst, P. Bruno, and W. Wulfhekel, Phys. Rev. B **78**, 174404 (2008).

[22] O. O. Shvetsov, V. D. Esin, A. V. Timonina, N. N. Kolesnikov, and E. V. Deviatov, Europhys. Lett. **127**, 57002 (2019)

[23] J. A. Hutasoit, J. Zang, R. Roiban, and C.-X. Liu, Phys. Rev. B **90**, 134409 (2014).

[24] S. S.-L. Zhang, A. A. Burkov, I. Martin, and O. G. Heinonen, Phys. Rev. Lett. **123**, 187201 (2019).

[25] J. Jiang, F. Tang, X. C. Pan, H. M. Liu, X. H. Niu, Y. X. Wang, D. F. Xu, H. F. Yang, B. P. Xie, F. Q. Song, P. Dudin, T. K. Kim, M. Hoesch, P. K. Das, I. Vobornik, X. G. Wan, and D. L. Feng, Phys. Rev. Lett. **115**, 166601 (2015).

[26] D. Rhodes, S. Das, Q. R. Zhang, B. Zeng, N. R. Pradhan, N. Kikugawa, E. Manousakis, and L. Balicas, Phys. Rev. B **92**, 125152 (2015).

[27] Y. Wang, K. Wang, J. Reutt-Robey, J. Paglione, and M. S. Fuhrer, Phys. Rev. B **93**, 121108(R) (2016).

[28] D. Kurebayashi and N. Nagaosa, Phys. Rev. B **100**, 134407 (2019).

[29] P. O. Sukhachov, M. V. Rakov, O. M. Teslyk, and E. V. Gorbar, Ann. Phys. (Berlin) **532**, 1900449 (2020).

[30] Y. Araki, Ann. Phys. (Berlin) **532**, 1900287 (2020).

[31] Y. Araki and K. Nomura, Phys. Rev. B **93**, 094438 (2016).

[32] E. B. Borisenko, V. A. Berezin, N. N. Kolesnikov, V. K. Gartman, D. V. Matveev, and O. F. Shakhlevich, Phys. Solid State **59**, 1310 (2017).

[33] A. Sidorov, A. E. Petrova, A. N. Pinyagin, N. N. Kolesnikov, S. S. Khasanov, and S. M. Stishov, JETP **122**, 1047 (2016).

[34] M. N. Ali, J. Xiong, S. Flynn, J. Tao, Q. D. Gibson, L. M. Schoop, T. Liang, N. Haldolaarachchige, M. Hirschberger, N. P. Ong, and R. J. Cava, Nature (London) **514**, 205 (2014).

[35] H. Y. Lv, W. J. Lu, D. F. Shao, Y. Liu, S. G. Tan, and Y. P. Sun, Europhys. Lett. **110**, 37004 (2015).

[36] A. Kononov, O. O. Shvetsov, A. V. Timonina, N. N. Kolesnikov, and E. V. Deviatov, JETP Lett. **109**, 180 (2019).

[37] O. O. Shvetsov, V. D. Esin, A. V. Timonina, N. N. Kolesnikov, and E. V. Deviatov, Phys. Rev. B **99**, 125305 (2019).

[38] A. Kononov, O. O. Shvetsov, S. V. Egorov, A. V. Timonina, N. N. Kolesnikov, and E. V. Deviatov, Europhys. Lett. **122**, 27004 (2018).

[39] J. C. Slonczewski, J. Magn. Magn. Mater. **159**, L1 (1996).

[40] G. Müller, D. Weiss, A. V. Khaetskii, K. von Klitzing, S. Koch, H. Nickel, W. Schlapp, and R. Lösch, Phys. Rev. B **45**, 3932(R) (1992).

[41] A. Würtz, R. Wildfeuer, A. Lorke, E. V. Deviatov, and V. T. Dolgopolov, Phys. Rev. B **65**, 075303 (2002).

[42] E. V. Deviatov, A. Ganczarczyk, A. Lorke, G. Biasiol, and L. Sorba, Phys. Rev. B **84**, 235313 (2011).

[43] A. Jash, Kamalika Nath, T. R. Devidas, A. Bharathi, and S. S. Banerjee, Phys. Rev. Applied **12**, 014056 (2019).

[44] A. Kononov, V. A. Kostarev, B. R. Semyagin, V. V. Preobrazhenskii, M. A. Putyato, E. A. Emelyanov, and E. V. Deviatov, Phys. Rev. B **96**, 245304 (2017).